
Learning to Initiate and Reason in Event-Driven Cascading Processes

Yuval Atzmon^{*1} Eli A. Meirum^{*1} Shie Mannor¹² Gal Chechik¹³

Abstract

Training agents to control a dynamic environment is a fundamental task in AI. In many environments, the dynamics can be summarized by a small set of events that capture the semantic behavior of the system. Typically, these events form chains or cascades. We often wish to change the system behavior using a single intervention that propagates through the cascade. For instance, one may trigger a biochemical cascade to switch the state of a cell or, in logistics, reroute a truck to meet an unexpected, urgent delivery. We introduce a new supervised learning setup called *Cascade*. An agent observes a system with known dynamics evolving from some initial state. The agent is given a structured semantic instruction and needs to make an intervention that triggers a cascade of events, such that the system reaches an alternative (counterfactual) behavior. We provide a test-bed for this problem, consisting of physical objects. We combine semantic tree search with an event-driven forward model and devise an algorithm that learns to efficiently search in exponentially large semantic trees. We demonstrate that our approach learns to follow instructions to intervene in new complex scenes. When provided with an observed cascade of events, it can also reason about alternative outcomes.

1. Introduction

Teaching agents to understand and control their dynamic environments is a fundamental problem in AI. It becomes extremely challenging when events trigger other events. We denote such processes as *cascading processes*. As an example, consider a set of chemical reactions in a cellular pathway. The synthesis of a new molecule is a discrete

^{*}Equal contribution ¹NVIDIA Research, Israel ²Technion, Israel institute of technology ³Bar Ilan University, Israel. Correspondence to: Yuval Atzmon <yatzmon@nvidia.com>, Eli Meirum <emeirum@nvidia.com>.

event that later enables other chemical reactions. Cascading processes are also prevalent in man-made systems: In assembly lines, when one task is completed, e.g., construction of gears, it may trigger another task, e.g. building the transmission system.

Cascading processes are abundant in many environments, from natural processes like chemical reactions, through managing crisis situations for natural disasters (Zuccaro et al., 2018; Nakano et al., 2022) to logistic chains or water treatment plants (Cong et al., 2010). A major goal with cascading processes is to intervene and steer them towards a desired goal. For example, in biochemical cascades, one tries to control chemical cascades in a cell by providing chemical signals; in logistics, a cargo dispatch plan may be completely modified by assigning a cargo plane to a different location.

This paper addresses the problem of reasoning about a cascading process and controlling its qualitative behavior. We describe a new counterfactual reasoning setup called “*Cascade*”, which is trained via supervised learning. At *inference* time, an agent observes a dynamical system, evolving through a cascading process that was triggered from some initial state. We refer to it as the “unsatisfied” or “observed” cascade. The goal of the agent is to steer the system toward a different, counterfactual, configuration. That target configuration is given as a set of qualitative constraints about the end results and the intermediate properties of the cascade. We call these constraints the “instruction”. To satisfy that instruction, the agent may intervene with the system at a *single, specific point in time* by changing the state of one specific element (the “pivot”).

To solve the *Cascade* learning problem, we train an agent to select an intervention given a state of a system and an instruction. Importantly, we operate in a counterfactual setup (See Pearl, 2000). During training, the agent only sees scenarios that are “satisfied”, in the sense that the system dynamics obey the constraints given in the instruction. The reason is that in the real world it is not possible to rewind time and simultaneously obtain both a satisfied and an unsatisfied sequence of events.

Steering a cascading process is hard. In many cascading processes, a slight change in one part of the system can make a qualitative effect on the outcome. This may lead to

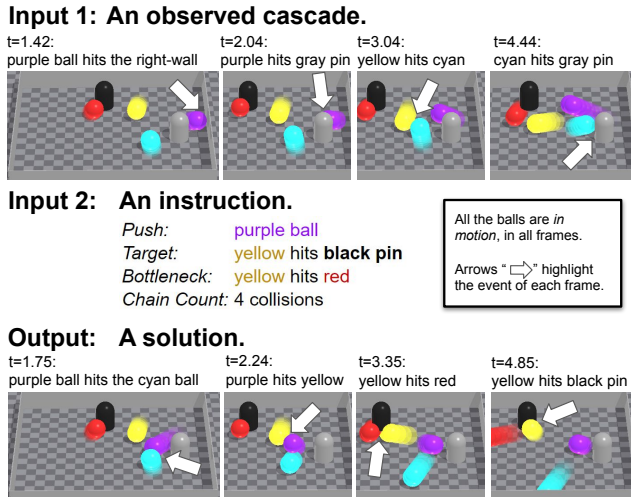


Figure 1. An experimental test bed for the *Cascade* setup. **Input 1** (the unsatisfied cascade): A set of balls is observed moving in a confined space, colliding with each other, with walls, and with static pins (grey & black). Collisions yield a cascade of events (arrows). **Input 2**: A complex instruction describes a desired “counterfactual” cascade of events and its constraints. **Output** (the satisfied cascade): The agent intervenes and sets the (continuous, 2D) initial velocity of the purple ball (the “pivot”) to achieve the goal, *satisfying the constraints*. Only keyframes are shown. See full videos here: <https://youtu.be/u1Io-ZWC1Sw> (Anonymous)

an exponential number of potential cascades. This “butterfly effect” (Lorenz, 1993) is typical in cascading systems, like a billiard ball missing another ball by a thread or a truck reaching a warehouse right after another truck has already left.

Consider a natural but naive approach to the Cascade problem: train an end-to-end regression model that takes the system and instruction as input and predicts the necessary intervention. We empirically find that this approach fails, presumably because the set of possible chains of events is exponentially large, and the model fails to learn how to find an appropriate chain that satisfies the instruction. We discuss other challenges in Section 4.

Technical insights. In designing our approach, we follow two key ideas. First, instead of modeling the continuous dynamics of the system, we reduce the search space by focusing on a small number of discrete, semantic events. To do this, we design a representation called an “*Event Tree*” (Figure 2). In a billiard game, these events would be collisions of balls. In logistic chains, these events would be deliveries of items to their target location or assembly of parts. To reduce the search space, we build a tree of possible future events, where the root holds the initial world-state. Each child node corresponds to a possible future subsequent semantic event from its parent. Thus, a path in the tree

from a root to a descendant captures a realizable sequence of events.

Our second idea is to learn how to efficiently search over the event tree. This is critical because the tree grows exponentially with its depth. We learn a function that assigns scores to tree nodes conditioned on the instruction and use these scores to prioritize the search. We also derived a Bayesian correction term to guide the search with the observed cascade: we first find the path in the event tree that corresponds to the observed cascade, and then correct the scores of nodes along that path.

Modelling system dynamics with forward models. A forward model describes the evolution of the dynamic systems in small time steps. There is extensive literature on learning forward models from observations in physical systems (Fragkiadaki et al., 2016; Battaglia et al., 2016; Lerer et al., 2016; Watters et al., 2017; Janner et al., 2019). Recent work also studied learning forward models for cascades (Qi et al., 2021; Girdhar et al., 2021). However, once the forward model has been learned, the desired initial condition of the system is found by an exhaustive search. Here, we show that exhaustive search fails for complex cascades and with semantic constraints (Section 4). Therefore, our paper focuses on *learning to search*, rather than on *learning the forward model*. We assume that we are given a special kind of a “forward” model operating at the level of semantic events. Namely, given a state of the cascading system, our forward model allows to query for the next event (“which objects collide next?”), and predict the outcome of that event (velocities of objects after collision).

Test bed. We designed a well-controlled environment that shares key ingredients with real-world cascading processes. In our test-bed several spheres move freely on a table, colliding with each other and with static pins within a confined space (Figure 1). The chain of collisions forms a complex cascading process. Naturally, a simulated test-bed cannot cover the full complexity of real-world scenarios and additional research may be required. We discuss these topics in Section 7.

Contributions. This paper proposes a novel approach for learning to *efficiently search* for a complex cascade in a dynamical system. Our contributions are: (1) A new learning setup, *Cascade*, where an agent observes a dynamical system and then changes its initial conditions to meet a given semantic goal. (2) Learning a principled probabilistic scoring function over a semantic *Event Tree*, for searching efficiently over the space of interventions. (3) A Bayesian formulation leveraging the observed cascade to guide the search in the event tree toward a counterfactual outcome.

2. The “Cascade” learning setup

Cascade is a supervised learning problem. At the *inference* phase, The agent is provided with a dynamical system and two inputs: (1) A sequence of events called the “observed cascade” together with the respective initial condition of the system. (2) An instruction that describes desired semantic properties (“constraints”) of the solution. The observed cascade does not satisfy the instruction. The agent is asked to intervene by controlling the state of one “pivot element” in the system at a specific point in time. The goal is to find an intervention that makes the roll out of the dynamical system satisfy the instruction.

At the *training* phase, we are *only given* “successful” labeled samples. Each sample consists of (1) an instruction; and (2) the initial state of the system except the controllable pivot. The “label” (y) of each sample is the initial state of the pivot, which yields the desired behavior of the system. During training we do not provide examples of failing sequences together with a successful sequence. The reason is that in reality, one cannot “roll-back” time and obtain both a failed sequence and a successful sequence.

More formally, our training set \mathcal{D} consists of N labelled samples $\mathcal{D} = \{\text{features} = (x_n, g_n), \text{label} = (y_n^*, Q(y_n^*)), n = 1 \dots N\}$, where:

- x_n is the initial state of a dynamical system, excluding those of its pivot element.
- $g_n \in \mathbb{R}^G$ is a structured representation of an instruction.
- $y_n^* \in \mathcal{Y} \subset \mathbb{R}^d$ is the pivot’s initial state of the solution.
- $Q(y_n^*) = \{s_k\}_{k=1}^K$ is a sequence of events that occur when the system is played out with the pivot initial value y_n .

At *test time*, a novel sample is drawn, describing an unseen dynamical system and instruction (x, g) ; and an observed cascade roll-out $(y^{obs}, Q(y^{obs}))$ which fails to fulfill the instruction. Our goal is to provide an alternative (counterfactual) initial state for the pivot element \hat{y} , such that the instruction is fulfilled when the system is rolled-out.

Our test bed: We introduce a new simulated test bed that abstract away from specific applications. An agent observes a physical world with several moving and static objects going through a cascade of events (Figure 1 top), and it is given a *complex* instruction “Push: purple ball ...”. It then manipulates the direction and speed of the purple ball (Figure 1 bottom) manifesting a new cascading process that satisfy the complex set of constraints given by the instruction. In the *Cascade* setup, the agent is trained on a set of scenes and their goals, and is tested on new scenes and their goals.

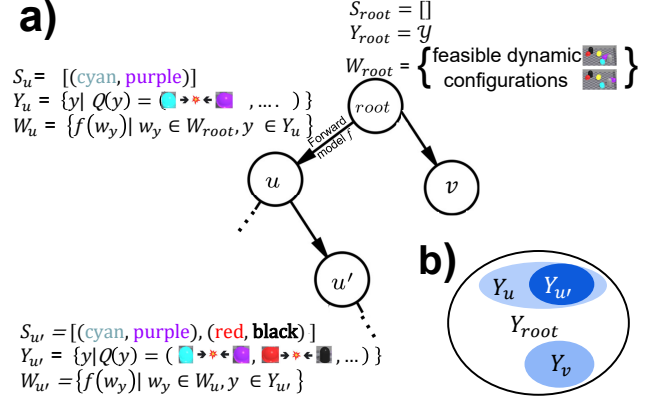


Figure 2. (a) The *Event Tree* data structure, illustrated according to our test-bed. S is the collision sequence of a node; Y is the intervention subset of a node; W is the node’s world-state. See Section 3.1. (b) Tessellation of the intervention space.

3. Methods

Solving the Cascade setup poses three major challenges. First, our model needs to identify semantic events, but simulations of dynamical systems typically follow fixed and small timesteps, which are indifferent to events. Second, the set of desired constraints and dynamical systems is compositional and large. The agent should learn to generalize to different systems and configurations that were not observed during training. Third, we wish to benefit from the example of the failed cascade that is only available at inference time (the counterfactual setup).

We develop an approach that addresses these three challenges. To address the first, we develop a representation that focuses on key “semantic” events of the dynamics (e.g., collisions). We build a tree of possible outcomes such that a path in the tree captures a realizable cascade of events. To address the second challenge, we learn a scoring function that assigns values to tree nodes conditioned on the instruction. This allows us to generalize to unseen setups, and at inference time, we use the predicted scores to search efficiently over the space of interventions. To address the third challenge, We develop a Bayesian formulation that allows to integrate the “counterfactual” information with the score predictions. Next, we describe each component in more detail.

3.1. The *Event Tree*: A tree of possible futures

We now describe the main data structure that we use to represent the search problem - the *Event Tree*. The event tree is designed to provide a searchable data structure for realizable sequences of events. To make these searches efficient, we represent the system behavior at the *semantic* level. These could be any key interactions between system components, like manufacturing an item in supply chains,

or a protein binding the DNA to regulate the expression of a gene. Importantly, in our approach, we require that it is possible to compute the state of the system right after an event.

Each node corresponds to a *sequence* of semantic events. The node’s children correspond to realizable continuations of the event sequence. Namely, all possible events that could happen after the sequence S_u . We now formally describe the node properties and the expansion of the event tree.

Tree Nodes. In the event tree, each node represents a subset of interventions $Y_u \subset \mathcal{Y}$ that share the same sequence of preceding events. These preceding events are referred to as the node’s *prefix* of semantic events. Each node has a unique prefix, $S_u \triangleq (s_1, s_2, \dots, s_u)$. Although different interventions within a node result in the same prefix, they may have different subsequent events after the prefix.

The root node describes the set of possible interventions at $t = 0$ and its sequence of events S_{root} is empty. Its *intervention subset* is $Y_{root} = \mathcal{Y}$. See Figure 2, top.

We define w_y^u as the state of the system after it evolved from $y \in Y$ and yielded the sequence S_u . Then, a “world-state” of a *node* is defined as the set $W_u = \{w_y^u | y \in Y_u\}$.

Given the world state of a current node, we propose an *event-driven forward model* $f(\cdot)$. It takes as input a state w_y^u and outputs the next immediate semantic event. We parallelized it on a GPU to detect possible futures for the world state W_u . Appendix I describes the forward model in detail.

Node Expansion. Suppose we decide to expand node u . We apply the forward model $f(\cdot)$ to each $w_y^u \in W_u$. A new node u' is composed of all $f(w_y^u)$ that share a same next semantic event s' . The event sequence of the child node u' is $S_{u'} = \text{concat}(S_u, s')$; the intervention set is $Y_{u'} = \{y | Q(y) \text{ has prefix } S_{u'}\}$.

Expanding the tree can be viewed as a tessellation refinement of the intervention space \mathcal{Y} . At each step, we pick one cell and split it into multiple cells, where each child cell represents a different event that occurs after a shared sequence of events, represented by the parent cell.

If the tree is fully expanded, it covers all possible futures. However, expanding the whole tree is expansive, as it grows exponentially with its depth. In the next subsection, we discuss how one can learn a scoring function and use it to guide an efficient tree search.

3.2. Assigning and learning a scoring function for nodes

The number of nodes in such trees grows exponentially with the tree depth and exceeds billions of nodes even in our basic setup (Section 4). Therefore, an exhaustive search is

infeasible, and a search method must be devised. To search the tree for a node that satisfies the goal, we prioritize which node to expand by learning a *scoring* function that assigns scores for nodes, conditioned on the instruction g . There are three key challenges in learning a score function. First, we do not have ground-truth (target) scores for tree nodes, and it is unclear what would be an effective assignment of scores. Second, the training data contains only positive examples of correctly designed plans. Finally, we wish to leverage the information about the faulty observed cascade, but a faulty cascade is only observed during inference time.

To motivate our approach, consider the following naive approach to set target scores. For a given tree, let the “target” u^* be the node that represents the ground-truth sequence S_{u^*} . A natural choice for setting scores would be to set $V(u^*) = 1$, and set all other scores to zero (“*All-or-None*”). However, this provides little guidance for searching the tree, as no signal is provided until the search hits the target node. Instead, a desired property of the learning algorithm would be to guide the search by assigning monotonically increasing scores along the path from the root to u^* .

To address these three challenges we design a principled probabilistic approach for setting the score function. We train our model to predict the likelihood that a sample from Y_u , when rolled out, will satisfy the instruction g .

$$V(u) = \Pr(Q(y) \text{ satisfies } g | y \in Y_u, g). \quad (1)$$

Here, nodes on the path from the root to u^* are assigned *monotonically increasing* scores, as the tessellation gets finer and concentrates on Y_{u^*} . Additionally, this probabilistic perspective allows us to take a maximum-likelihood approach at inference time to prioritize nodes.

We use a sampling-based estimate of $V(u)$ to calculate the ground-truth scores for training. We take a finite sample of $\hat{Y}_{root} \subset \mathcal{Y}$, collecting say 10^6 points, and use it to expand the tree. The node’s score is then the fraction of the samples from \hat{Y}_u that reach the target node u^* .

$$\hat{V}(u) = \Pr(y_i \in \hat{Y}_{u^*} | y_i \in \hat{Y}_u, g) = \frac{\|\hat{Y}_{u^*} \cap \hat{Y}_u\|}{\|\hat{Y}_u\|}. \quad (2)$$

Nodes outside that sequence get a score of 0. In Section 4, we empirically explore alternative approaches for assigning ground-truth scores to nodes.

Counterfactual update for the score function. During inference, we observe a cascade that does not satisfy the instruction, and are asked to retrospectively suggest a better solution. How can the observed cascade be used to find a solution? The probabilistic score function we defined allows us to formalize this problem in a Bayesian setting. We treat the model predictions as a *prior* for the true score, and the information about the observed cascade as *evidence*. We then ask how to update the score function given the observed

evidence. Formally, our goal is to solve Eq. (1) when it is conditioned by the evidence, $V(u|S_{u^{obs}}$ doesn't satisfy g).

During training, our model learns to estimate the *unconditioned* score function $V(\cdot)$. In the appendix, we show that we can express the Bayesian update of the scores in terms of $V(u^{obs}), V(u)$,

$$V(u|S_{u^{obs}} \text{ doesn't satisfy } g) = V(u) - V(u^{obs}) \cdot fr(y^{obs}, y_u). \quad (3)$$

where $fr(u^{obs}, u) = \Pr(y \in Y_{u^{obs}} | y \in Y_u)$ is the probability that an intervention $y \in Y_u$ will result in sequence with prefix $S_{u^{obs}}$. It is estimated in a fashion similar to Eq. (2).

A model for the score function. Next, we describe the representation and architecture for modelling the score function. The model takes as inputs the instruction g and sequence of events S_u that define the node u , and predicts a scalar score with ground-truth labels according to Eq. (2).

A naive approach is to represent S_u as a sequence. However, such representation may not convey well the relations describing the cascade of events. For illustration, in the following sequence of collision events $[(A, B), (C, D), (A, E)]$, the collision (A,E) is driven by (A,B), because A is common for both, while (C,D) is less relevant for describing the events that lead to (A,E). Instead, we transform each sequence to a Directed Acyclic Graph (DAG) that captures relations in the cascade of events. A node in this DAG is an event that involves some elements. Each edge represents an element shared by two subsequent events. See Figure 3 for a concrete illustration.

Architecture We use a Graph Neural Network (GNN) to parameterize our score function. We represent the graph as a tuple (A, X, E, z) where $A \in \{0, 1\}^{n \times n}$ is the graph adjacency matrix, $Y \in \mathbb{R}^{n \times d}$ is a node feature matrix, $E \in \mathbb{R}^{m \times d'}$ is an edge feature matrix, and $z \in \mathbb{R}^{d''}$ is a global graph feature. We chose to use a popular message passing GNN model (Battaglia et al., 2018). We describe its architecture in detail in the appendix.

3.3. Inference

Our agent searches the tree for the maximum scored node u_{MAX} . Then, it randomly selects an intervention from its intervention subset $y \in Y_{u_{MAX}}$. We consider two variants.

Maximum likelihood search: The agent performs a tree search that expands the most likely nodes. At any given step, the agent stores a sorted list of nodes together with their likelihood scores, it then picks the highest scoring node from this list and expands it. The node children are then added to the list with their predicted scores, and the agent resorts the list.

We limit the tree search to expand only 80 nodes, whereas in our test bed a full event tree, which contains all possible

$S = [(cyan, purple), (red, black), (yellow, purple), (red, yellow), (purple, gray), (cyan, wall), (yellow, black), \dots]$

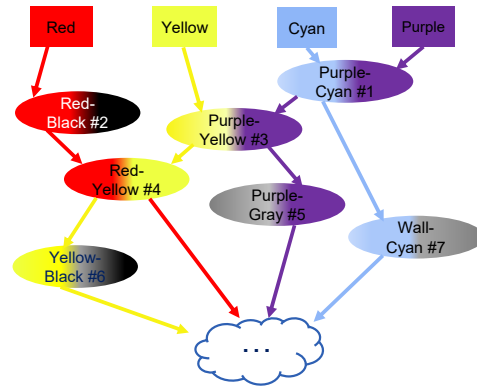


Figure 3. Illustrates transforming a sequence of events (top) to a DAG (bottom). It corresponds to the video in Figure 1 bottom.

realizations, have billions of nodes, $\sim \times 2.8$ per unit of depth (empirically).

Counterfactual search: Here we explain how we leverage the information in the *observed* cascade for inference. Consider the case where the sequence of the solution is complex and the observed sequence diverges from the solution at a late point. In this case, it is likely that a part of the observed chain will be informative about the solution, and will diverge at some point. To use that information, we apply the Bayesian correction (Eq. 3) term to the predicted score of every node along the observed sequence. We pick the highest scoring node, and initialize the search up to that node. Then we continue the search as described by the “Maximum likelihood search”. In practice, we trim the observed sequence, at $N_{observed}$ nodes. $N_{observed}$ is a hyper-parameter.

4. Experiments

We compared our approach to state-of-the-art baselines, including human performance. Then, we follow with an ablation study to examine the contributions of different components in our approach. Next, we describe our experimental protocol, compared methods, and evaluation metrics.

4.1. A simulation benchmark

We created a well-controlled environment that closely mimics the key characteristics of real-world cascading processes.¹ This environment has been designed to be: (1) sensitive to initial conditions, allowing a wide range of future cascades, (2) contain diverse scenes, each representing a unique dynamical system. (3) incorporate semantic goals that depend on intermediate outcomes; and (4) capable of benchmarking counterfactual scenarios.

¹Examples: [link #1](#), [link #2](#), [link #3](#).

Scenes. In our test-bed, several spheres move freely on a frictionless table, colliding with each other and with static pins within a confined four-walled space (Figure 1). Each episode describes a different scene, which includes tens of collisions.

Instructions. A structured instruction describes (i) A pivot element to manipulate “*Push: green ball*”; (ii) A target semantic event (collision) to fulfill “*Target: red hits black pin*”; and (iii) constraints, of two possible types. First, is a “count” constraint. It resembles constraining the total amount of resources available on a logistic chain. It specifies an accumulated number of collisions, on *all* the paths from the pivot to the target, e.g. “*Chain Count: 3*”. Second, is a “bottleneck” constraint, which resembles a bottleneck along a logistic chain. It enforces a specific collision to occur before the target collision, e.g. “*Bottleneck: red hits top wall*”. The appendix describes the instruction generation process with more examples.

The task. The agent’s objective is to intervene with the initial state of the scene by setting the velocity of the pivot object, in order to cause a set of collisions described in the instruction. This often requires a precise “trick shot”, that requires careful reasoning about how the subsequent events will unfold. **Dataset.** We generated a dataset with $\sim 46K$ scenes (we limited generation time to 80 hours), each includes 4-6 moving balls, 0-2 pins, and 4 walls and up to 5 semantic instructions (~ 4.25 on average). The data is split by unique *scenes*, into 470 unseen scenes for test, 69 scenes for selecting hyper-parameters (val. set), and the rest are used for training. See Appendix H for more details.

4.2. Experiment details

Compared Methods: We compared the following methods. **(1) ROSETTE (Reasoning On SEmanTic TREs):** Our approach described in Section 3. Search uses the “counterfactual” variant of the tree search (Section 3.3), by first expanding the nodes along the “observed” sequence. **(2) ROSETTE-max-l:** Like #1, but using “Maximum likelihood search” (Section 3.3) - not using the “observed” sequence. For a fair comparison, we make sure that ROSETTE expands the same number of nodes in total as ROSETTE-max-l. **(3) (Qi et al., 2021),** The SOTA on PHYRE, based on a learned forward model, goal-satisfaction classifier and exhaustive search. For a fair comparison we replace their learned forward model by the full simulator of Makovychuk et al. (2021). Hence, this baseline benefitted from using an exact forward model. **(4) Cross Entropy:** A standard planner (de Boer et al., 2005; Greenberg et al., 2022) that optimizes the objective function learned by compared method (3). Similarly to (3), this baseline had access to the exact model. **(5) Sequential:** Using a sequential representation for a tree chain, instead of a DAG. Specifically, we represent the sequence as a graph with edges along the sequence.

(Litany et al., 2022) compared a recurrent versus standard synchronous propagation in GNN models and found them empirically equivalent. **(6) Deep Sets regression:** Embedding the instruction and the initial world state to predict a continuous intervention. We embed the objects’ initial positions and velocities using the permutation-invariant “Deep Sets” architecture (Zaheer et al., 2017), and use an L_2 loss with respect to ground-truth interventions in the “counterfactual” training samples. **(7) Random:** Sample interventions at random from an estimated distribution of ground-truth interventions. Details appear in the appendix.

Ablation: We also carry a thorough ablation study: First, we explore alternative approaches to label node scores along the ground-truth sequence. *Linear:* Linearly increases the score by $V(u) = depth(u)/depth(u^*)$. *Step:* Give a fixed medium score to nodes along the sequence, and a maximal score to the target node: $V(u) = 0.5 + 0.5\mathbf{1}_{u^*}(u)$. *All-or-None:* Sets $V(u) = \mathbf{1}_{u^*}(u)$, this baseline is equivalent to the naive approach discussed in Section 3.2. Second, we compare the “Counterfactual” search to the “Maximum Likelihood” search by comparing their performance on **a dataset that includes more complex instructions**. This dataset includes a third constraint. We partition the dataset to “Easy” and “Hard” instructions, and compare these search methods on both types of instructions. We describe this dataset in the appendix. Third, we assess the impact of varying “levels” of diverging points on overall performance when presented with an observed cascade. Specifically, we aimed to quantify the benefits of the counterfactual update in situations where the observed sequence diverges from the solution at a later point. Last, we test how ablating parts of the instruction affects the ROSETTE model performance. Implementation details of the baselines and ablations are described in Section D.

	TREE SUCCESS	SIMULATOR SUCCESS
RANDOM	NA	$17.6 \pm 0.3\%$
DEEPPSET REGRESSION (QI ET AL., 2021)	NA	$18.4 \pm 0.5\%$
CROSS ENTROPY	NA	$21.1 \pm 0.9\%$
SEQUENTIAL	$52.4 \pm 0.6\%$	$20.9 \pm 0.4\%$
ROSETTE (OURS)	$60.8 \pm 0.3\%$	$48.8 \pm 0.3\%$

Table 1. **Success rates** of Our approach and baselines. TREE is not applicable to the first three baselines since they do not use an event tree.

	TREE SUCCESS
ALL-OR-NONE	$33.5 \pm 1.6\%$
STEP	$45.1 \pm 1.0\%$
LINEAR	$48.7 \pm 0.7\%$
ROSETTE-MAX-L (OURS)	$59.7 \pm 0.3\%$

Table 2. **Success rates** of the score function variants (see Ablation).

# DIVERGE	ROSETTE	ROSETTE-MAX-L	N
≤ 2	$55.4 \pm 0.6\%$	$55.5 \pm 0.6\%$	6750
3...4	$58.9 \pm 1.1\%$	$54.2 \pm 1.1\%$	2435
5+	$50.4 \pm 1.2\%$	$44.5 \pm 1.2\%$	1765

Table 3. The impact of varying levels of diverging points from the observed cascade on overall performance (see Ablation). The counterfactual update didn’t provide a significant advantage for early diverging points (≤ 2). However, it did result in a noteworthy 13% increase in success rate for later diverging points (50.4% vs 44.5%).

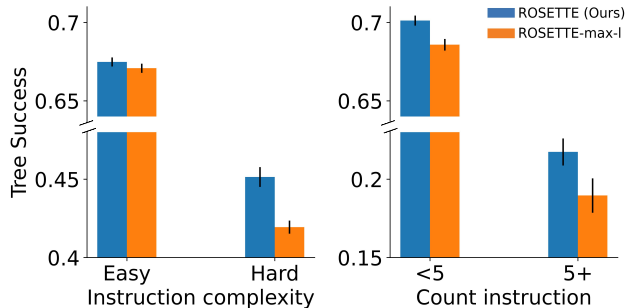


Figure 4. Comparing “Counterfactual” search (ROSETTE) with “Maximum likelihood” search (ROSETTE-max-l) for 2 levels of instruction complexity (“Hard”: 2 or more constraints) and for two levels of “count” instructions (“5+”: 5 or more). Using the observed cascade, ROSETTE performs better in complex scenarios.

Evaluation metrics: For each episode and goal, we predict an intervention and evaluate their success rate using the following metrics. **Simulator success rate:** The success rate when rolling out the predicted intervention using a physical simulator (Makovychuk et al., 2021). This metric mimics experimenting in the real world. **Tree success rate** (where applicable): Each node in the tree represents a sequence of events. A tree based algorithm selects a node. A “tree success” is when the selected node’s sequence satisfy the instruction. This metric evaluates the performance of the score function and tree search, independently from errors that may be introduced due to the event-driven forward model.

We further measured refinements of these metrics by conditioning on various properties of the instruction and scene. **(1) Condition tree success rate on instruction type: Unconstrained:** The instruction only specifies target collisions. **Bottleneck:** also contains an “bottleneck” constraint. **Count:** contains a “count” constraint. **B&C:** contains both “bottleneck” and “count” constraints. **(2) Condition tree success rate on complex scenarios:** (2.1) Instructions with 2 or more constraints are marked as “Hard”, and the rest as “Easy”; (2.2) Instructions with a “count” constraint value ≥ 5 are considered hard. Complex scenario conditioning was evaluated on the complex instruction dataset. Using the main dataset demonstrate a similar trend (See appendix K).

We report mean value and standard error of the mean across 5 model seeds.

4.3. Human evaluation

To assess a human baseline, we conducted a user study with Amazon Mechanical Turk. We designed a game, where a player is given a video of the observed cascade and is asked to select one of 44 combinations of orientations (11) and speeds (4). The game is based on 30 test episodes. For comparing with ROSETTE, we select the one (of 44) which is nearest (in L_2) to ROSETTE’s predicted velocity. Appendix C, describes the experiment design and further analysis of the results.

5. Results

We first compare the performance of ROSETTE with baseline methods and human performance. We then study its properties in greater depth, through a series of ablation experiments. We discuss the baselines’ results in Appendix A.1, and we provide qualitative examples in Appendix B.

Table 1 describes the *Tree* and the *Simulator* success rates of ROSETTE and compared methods. ROSETTE achieves the highest success rate for both the “Tree” success rate (60.8%) and the “Simulated” success rate (48.8%). Achieving $\sim 80\%$ conversion rate from *Tree* to *Simulated*. The random baseline success rate is (17.6%), which is close to the performance of the regression model. We conjecture that the regression model fails, because it can’t represent the outcomes as ROSETTE can. The Sequential approach is the strongest baseline, reaching $Tree = 52.4\%$ and $Simulated = 43.1\%$ success rates.

In the human study, ROSETTE achieves the highest average success rate ($43.3\% \pm 1.3\%$ vs $23.9\% \pm 2.6\%$). Humans displayed a large range of success rates, ranging from 10% to 41.4%, with a median of 25%. ROSETTE performed more persistent, with 46.6%, 43.3% and 40% for the best, median, and worst.

Ablation experiments: We highlight some key observations. **(1)** Table 2 shows the advantage of the probabilistic formulation of the score function (ROSETTE-max-l), compared to the several heuristics described in Section 4. The strongest baseline (“Linear”) only reaches 48.7% vs. 59.7% for ROSETTE-max-l. **(2)** The *All-or-None* variant *establishes the value of event-drivenness*. It is similar to a classifier-based search like (Qi et al., 2021), but uses an underlying event-driven forward model instead of a fixed time stamp model as in (Qi et al., 2021). Comparing the two, we see that using EDFM with current SOTA improves the success rate, from 21% to 33.5%. **(3)** Comparing *ROSETTE-max-l* to the *All-or-None* variant further *establishes value of learning to search*, which improves the success rate

from 33.5% to 59.7%. (3) Figure 4 quantifies the benefit gained by using “Counterfactual” search (ROSETTE) over Maximum-Likelihood search (Section 3.3). ROSETTE shows a relative improvement of 7.7% (45.1% vs 41.9%) for complex instructions. (4) Table 3 examines how different levels of diverging points affect performance. Early diverging points (≤ 2) don’t benefit from the counterfactual update. However, later diverging points result in a 13% relative improvement in success rate with the counterfactual update (50.4% vs 44.5%). (5) Table 4 (Appendix A) allows an in-depth examination of the strengths and weaknesses of ROSETTE, across 4 types of ablations, as described in Section 4. First, we observe that the sequential baseline can find target collisions that depend on a bottleneck collision, as well as ROSETTE. However, it fails with “count” instructions (46.3% vs 60.8%), since it has no capacity for that reasoning task. Second, we observe that ROSETTE is able to effectively use the instruction, as removing any part of the instruction hurts the success rate.

6. Related work

Learning and reasoning in physical systems. Several papers studied cascading events in the context of physical systems. There, the main focus was to use object interactions to learn a forward model from observations. PHYRE, Virtual Tools, and CREATE (Bakhtin et al., 2019; Allen et al., 2020; Jain et al., 2020) are benchmarks for physical reasoning for computer vision. They differ from our learning setup in three key aspects. First, the current paper focuses on the *search* problem, looking to satisfy a set of semantic constraints on the event sequence. Second, in the prior benchmarks, all tasks have to satisfy the same final goal, rather than being conditioned on a semantic goal. Last, their setup is a sequential decision reinforcement learning setup, allowing exploration, collecting rewards from the environment, and multiple retries, which are not allowed in our setup. In addition, no event-driven forward model (EDFM) is currently available for these benchmarks, and training an EDFM requires additional annotations and is beyond the scope of this work. There are several approaches to learn such models from temporal data, like dynamic Bayes nets (Bhattacharjya et al., 2020; Ghahramani, 1998; Gunawardana & Meek, 2016), which can also handle latent variables.

Allen et al. (2020) takes a Bayesian approach for updating the distribution of initial conditions given a reward. We consider the underlying chain of events and update the value of the node scores in the event tree according to the observed cascade. CLEVRER, CoPhy, CRAFT, CATER, and IntPhys (Yi et al., 2020; Baradel et al., 2020; Ates et al., 2021; Girdhar & Ramanan, 2020; Riochet et al., 2018) are benchmarks for reasoning over observed temporal and causal structures

in video. They differ from our setup in a few key aspects: (1) They focus on video-tracking and question answering rather than acting. (2) In CLEVRER and CoPhy, the observed cascade is available during training, which may not be a reasonable assumption for real-world problems (see Section 2). (3) CoPhy estimates the value of a *static* observed property, like gravity, while we focus on the cascade evolution.

Roussel et al. (2019) studied the chain reaction problem, with a different focus than ours. Their cascading configuration is fully given and they study how to tune that configuration using a simulator. Our work focuses on *finding* a cascading configuration given a partial description of it.

Finally, reasoning about observed content in a new set of environments was studied by Agrawal et al. (2021). They focused on reasoning by elimination as a means of investigating the ability to make accurate inferences about never-before-seen objects or concepts. To construct the reasoning policy, they employed reinforcement learning.

Graph Neural Networks have been used in physical environments (Kim & Shimanuki, 2019; Shen et al., 2020; Bapst et al., 2019), representing the underlying state as a graph, without considering temporal consequences. Temporal consequences are vital for our decision system. We propose how to transform a *temporal sequence* of events to a DAG.

Reinforcement learning: The “Cascade” learning setup is fundamentally different from a reinforcement learning framework (Sutton & Barto, 2005). The problem we try to solve is not a standard planning problem (Hafner et al., 2019), where a series of actions are taken sequentially. Here, an action is taken once and sets the cascade of events (“Fire and forget”).

Our problem shares similarities with the problem of evaluating a Markov Reward Process (MRP). Instead of looking at individual physical states, we group them into *sets* based on a common sequence of semantic events that led to them. In Appendix L we define an MRP reward function and demonstrate that this reward function induces a value function that is aligned with our score function. Nevertheless, our approach has the advantage of directly learning the score (value) function, by leveraging the problem’s structure. Additionally, we can naturally incorporate counterfactual information into the cascading process structure.

Our problem can also be posed as a contextual bandit problem (Bouneffouf et al., 2020). However, this does not offer an algorithm that will allow us to benefit from the counterfactual information and the cascading process structure.

Monte Carlo tree search approaches (Chaslot et al., 2008) build a search tree by stochastic tree expansions and evaluate the outcomes. In our approach, we construct an auxiliary structure (the “event-tree”) to support our planning algo-

rithm. Expanding the event tree refines (tessellates) the intervention set. In contrast, expanding the tree in MCTS represents an interaction with the environment (“action”). This interaction involves a reward, a new state, and a new chance to interact with the environment. All of these are not present in our setup. Our approach shares some similarities with MuZero (Schrittwieser et al., 2020) as both approaches use a forward model to simulate a node’s semantic representation based on its parent’s representation.

Our problem can also be posed as a contextual bandit problem, this does not offer an algorithm that will allow us to benefit from the counterfactual information and the cascading process structure.

Planning in robotics: Pertsch et al. (2020); Jayaraman et al. (2019) learned from video data to predict key-frames, conditioned on a start frame and an end frame (goal). These works rely on a visual end goal. It is unclear how to use them with a semantic goal that includes constraints. They also rely on taking multiple actions, which is not applicable in our “Fire and forget” setup.

Causal inference: Counterfactual reasoning was studied in causal inference (Pearl, 2000). Most relevant is (Buesing et al., 2019) that used counterfactually augmented data for training a RL policy.

Few-shot learning and Meta Reinforcement learning: The counterfactual setup we use is similar to a probabilistic perspective of few-shot learning (Fei-Fei et al., 2006; Samuel et al., 2020) and meta-learning (Greenberg et al., 2023; Ortega et al., 2019; Zintgraf et al., 2021; Rakelly et al., 2019), which aim to make decisions based on limited observations. However, there are two main differences. First, we cannot access training data to learn a meta-algorithm because we operate in a counterfactual mode. According to Pearl (2000), during training in a counterfactual mode, the agent only observes successful scenarios, as obtaining both satisfied and unsatisfied scenarios simultaneously in the real world is impossible. Second, the observed cascade is always a failure case, unlike successful examples used in traditional few-shot learning and meta-learning.

7. Discussion

In this paper, we took a first step towards understanding how to affect a complex system of cascading events. We presented a new learning setup, called *Cascade*, where an agent observes a cascade of events in a dynamical system and is asked to intervene and change its initial state to make the system meet a given goal. We use an event-tree representation and a principled probabilistic score function for searching efficiently over the space of interventions. We also describe an approach to counterfactually reason about an observed cascade during the tree search.

Our approach is best applied in problems that are naturally described by event-driven dynamics. As an example, consider cascading failures in power grids (Schäfer et al., 2018). Here, semantic events are failures of nodes (transformers, power generators, ...) or edges (power lines). The power flow obeys a known set of differential equations for a given grid. When flow exceeds a powerline capacity, that line fails (an event), resulting in an effectively different grid and a different set of equations that govern the dynamics. The transmission system operator may wish to define goals like “no more than three failures”, “no more than n people affected”, “that important node must not fail”. We elaborate on this use-case and other use-cases, such as logistics and evolution of natural disasters in Appendix J.

An important question remains: How do studies that use our toy testbed can generalize to real-world scenarios? We believe it can follow a similar paths as in other areas of AI where approaches mature from toy datasets to realistic problems: First, by creating a benchmark dataset for a real-world domain, annotated with semantic events. Some fields have datasets that can be very natural for the problem we discussed. These may include logistics (Appendix J), evolution of natural disasters and their consequences (Zuccaro et al., 2018), and cascading failures in power grids (Schäfer et al., 2018). Second, an event-driven forward model (EDFM) needs to be trained using this dataset. Domain specific properties can be used to improve the accuracy and robustness of an EDFM learned. Finally, given the EDFM, our approach can be applied.

References

- Agrawal, H., Meirom, E. A., Atzmon, Y., Mannor, S., and Chechik, G. Known unknowns: Learning novel concepts using reasoning-by-elimination. In *Conference on Uncertainty in Artificial Intelligence*, 2021.
- Allen, K. R., Smith, K. A., and Tenenbaum, J. B. Rapid trial-and-error learning with simulation supports flexible tool use and physical reasoning. *Proceedings of the National Academy of Sciences*, 117:29302 – 29310, 2020.
- Ates, T., Atesoglu, M. S., Yigit, C., Kesen, I., Kobas, M., Erdem, E., Erdem, A., Goksun, T., and Yuret, D. Craft: A benchmark for causal reasoning about forces and interactions, 2021.
- Bakhtin, A., van der Maaten, L., Johnson, J., Gustafson, L., and Girshick, R. B. Phyre: A new benchmark for physical reasoning. In *Advances in Neural Information Processing Systems (NeurIPS)*, 2019.
- Bapst, V., Sanchez-Gonzalez, A., Doersch, C., Stachenfeld, K. L., Kohli, P., Battaglia, P. W., and Hamrick, J. B. Structured agents for physical construction. In *ICML*, 2019.
- Baradel, F., Neverova, N., Mille, J., Mori, G., and Wolf, C. Cophy: Counterfactual learning of physical dynamics, 2020.
- Battaglia, P. W., Pascanu, R., Lai, M., Rezende, D., and Kavukcuoglu, K. Interaction networks for learning about objects, relations and physics. In *Advances in Neural Information Processing Systems (NeurIPS)*, 2016.
- Battaglia, P. W., Hamrick, J. B., Bapst, V., Sanchez-Gonzalez, A., Zambaldi, V., Malinowski, M., Tacchetti, A., Raposo, D., Santoro, A., Faulkner, R., Gulcehre, C., Song, F., Ballard, A., Gilmer, J., Dahl, G., Vaswani, A., Allen, K., Nash, C., Langston, V., Dyer, C., Heess, N., Wierstra, D., Kohli, P., Botvinick, M., Vinyals, O., Li, Y., and Pascanu, R. Relational inductive biases, deep learning, and graph networks, 2018.
- Bhattacharjya, D., Shanmugam, K., Gao, T., Mattei, N., Varshney, K. R., and Subramanian, D. Event-driven continuous time bayesian networks. In *AAAI*, 2020.
- Bouneffouf, D., Rish, I., and Aggarwal, C. Survey on applications of multi-armed and contextual bandits. In *2020 IEEE Congress on Evolutionary Computation (CEC)*, pp. 1–8. IEEE, 2020.
- Buesing, L., Weber, T., Zwols, Y., Heess, N., Racaniere, S., Guez, A., and Lespiau, J.-B. Woulda, coulda, shoulda: Counterfactually-guided policy search. In *International Conference on Learning Representations*, 2019. URL <https://openreview.net/forum?id=BJG0voC9YQ>.
- Chaslot, G., Bakkes, S., Szita, I., and Spronck, P. Monte-carlo tree search: A new framework for game ai. In *Proceedings of the AAAI Conference on Artificial Intelligence and Interactive Digital Entertainment*, volume 4, pp. 216–217, 2008.
- Cong, Q., Yu, W., and you Chai, T. Cascade process modeling with mechanism-based hierarchical neural networks. *International journal of neural systems*, 20 1:1–11, 2010.
- de Boer, P. T., Kroese, D. P., Mannor, S., and Rubinstein, R. Y. A tutorial on the cross-entropy method. *Annals of Operations Research*, 134:19–67, 2005.
- Fei-Fei, L., Fergus, R., and Perona, P. One-shot learning of object categories. *IEEE Transactions on Pattern Analysis and Machine Intelligence*, 28:594–611, 2006.
- Fragkiadaki, K., Agrawal, P., Levine, S., and Malik, J. Learning visual predictive models of physics for playing billiards, 2016.
- Ghahramani, Z. *Learning dynamic Bayesian networks*, pp. 168–197. Springer Berlin Heidelberg, Berlin, Heidelberg, 1998. ISBN 978-3-540-69752-7. doi: 10.1007/BFb0053999. URL <https://doi.org/10.1007/BFb0053999>.
- Girdhar, R. and Ramanan, D. Cater: A diagnostic dataset for compositional actions and temporal reasoning, 2020.
- Girdhar, R., Gustafson, L., Adcock, A., and van der Maaten, L. Forward prediction for physical reasoning. *Time Series Workshop, ICML*, 2021.
- Greenberg, I., Chow, Y., Ghavamzadeh, M., and Mannor, S. Efficient risk-averse reinforcement learning. In *Advances in Neural Information Processing Systems*, 2022.
- Greenberg, I., Mannor, S., Chechik, G., and Meirom, E. A. Train hard, fight easy: Robust meta reinforcement learning. *ArXiv*, abs/2301.11147, 2023.
- Gunawardana, A. and Meek, C. Universal models of multivariate temporal point processes. In *AISTATS*, 2016.
- Hafner, D., Lillicrap, T., Fischer, I., Villegas, R., Ha, D., Lee, H., and Davidson, J. Learning latent dynamics for planning from pixels. In *International Conference on Machine Learning*, pp. 2555–2565, 2019.
- Hagberg, A., Swart, P., and S Chult, D. Exploring network structure, dynamics, and function using networkx. Technical report, Los Alamos National Lab.(LANL), Los Alamos, NM (United States), 2008.

- Jain, A., Szot, A., and Lim, J. J. Generalization to new actions in reinforcement learning. In *ICML*, 2020.
- Janner, M., Levine, S., Freeman, W. T., Tenenbaum, J. B., Finn, C., and Wu, J. Reasoning about physical interactions with object-oriented prediction and planning. In *Proceedings of the International Conference on Learning Representations (ICLR)*, 2019.
- Jayaraman, D., Ebert, F., Efros, A., and Levine, S. Time-agnostic prediction: Predicting predictable video frames. In *International Conference on Learning Representations*, 2019. URL <https://openreview.net/forum?id=SyZVb3CcFX>.
- Kim, B. and Shimanuki, L. Learning value functions with relational state representations for guiding task-and-motion planning. In *CoRL*, 2019.
- Kingma, D. and Ba, J. Adam: A method for stochastic optimization. In *ICLR*, 2015.
- Lerer, A., Gross, S., and Fergus, R. Learning physical intuition of block towers by example, 2016.
- Litany, O., Maron, H., Acuna, D., Kautz, J., Chechik, G., and Fidler, S. Federated learning with heterogeneous architectures using graph hypernetworks, 2022.
- Lorenz, E. N. *The Essence of Chaos*. UCL Press, London, 1993.
- Makoviychuk, V., Wawrzyniak, L., Guo, Y., Lu, M., Storey, K., Macklin, M., Hoeller, D., Rudin, N., Allshire, A., Handa, A., and State, G. Isaac gym: High performance gpu-based physics simulation for robot learning, 2021.
- Nakano, R., Hirabayashi, M., Agrusa, H. F., Ferrari, F., Meyer, A. J., Michel, P., Raducan, S. D., Lana, D. P. S., and Zhang, Y. Nasa’s double asteroid redirection test (dart): Mutual orbital period change due to reshaping in the near-earth binary asteroid system (65803) didymos. *The Planetary Science Journal*, 3, 2022.
- Ortega, P. A., Wang, J. X., Rowland, M., Genewein, T., Kurth-Nelson, Z., Pascanu, R., Heess, N. M. O., Veness, J., Pritzel, A., Sprechmann, P., Jayakumar, S. M., McGrath, T., Miller, K. J., Azar, M. G., Osband, I., Rabinowitz, N. C., György, A., Chiappa, S., Osindero, S., Teh, Y. W., Hasselt, H. V., de Freitas, N., Botvinick, M. M., and Legg, S. Meta-learning of sequential strategies. *ArXiv*, abs/1905.03030, 2019.
- Pearl, J. *Causality: models, reasoning and inference*, volume 29. Springer, 2000.
- Pertsch, K., Rybkin, O., Yang, J., Zhou, S., Derpanis, K. G., Daniilidis, K., Lim, J. J., and Jaegle, A. Keyframing the future: Keyframe discovery for visual prediction and planning. In *Learning for Dynamics & Control Conference*, 2020.
- Qi, H., Wang, X., Pathak, D., Ma, Y., and Malik, J. Learning long-term visual dynamics with region proposal interaction networks. In *ICLR*, 2021.
- Rakelly, K., Zhou, A., Quillen, D., Finn, C., and Levine, S. Efficient off-policy meta-reinforcement learning via probabilistic context variables. 2019.
- Riochet, R., Castro, M. Y., Bernard, M., Lerer, A., Fergus, R., Izard, V., and Dupoux, E. Intphys: A framework and benchmark for visual intuitive physics reasoning. *ArXiv*, 2018.
- Roussel, R., Cani, M.-P., Léon, J.-C., and Mitra, N. J. Designing chain reaction contraptions from causal graphs. *ACM Trans. Graph.*, 38(4), 2019. ISSN 0730-0301. doi: 10.1145/3306346.3322977. URL <https://doi.org/10.1145/3306346.3322977>.
- Samuel, D., Atzmon, Y., and Chechik, G. From generalized zero-shot learning to long-tail with class descriptors. *2021 IEEE Winter Conference on Applications of Computer Vision (WACV)*, pp. 286–295, 2020.
- Schäfer, B., Witthaut, D., Timme, M., and Latora, V. Dynamically induced cascading failures in power grids. *Nature Communications*, 9, 2018.
- Schrittwieser, J., Antonoglou, I., Hubert, T., Simonyan, K., Sifre, L., Schmitt, S., Guez, A., Lockhart, E., Hassabis, D., Graepel, T., Lillicrap, T., and Silver, D. Mastering atari, go, chess and shogi by planning with a learned model. *Nature*, 588(7839):604–609, dec 2020. doi: 10.1038/s41586-020-03051-4. URL <https://doi.org/10.1038/s41586-020-03051-4>.
- Shen, W., Trevizan, F. W., and Thi’ebaux, S. Learning domain-independent planning heuristics with hypergraph networks. In *ICAPS*, 2020.
- Sutton, R. S. and Barto, A. G. Reinforcement learning: An introduction. *IEEE Transactions on Neural Networks*, 16: 285–286, 2005.
- Watters, N., Tacchetti, A., Weber, T., Pascanu, R., Battaglia, P., and Zoran, D. Visual interaction networks. In *Advances in Neural Information Processing Systems (NeurIPS)*, 2017.
- Yi, K., Gan, C., Li, Y., Kohli, P., Wu, J., Torralba, A., and Tenenbaum, J. B. Clevrer: Collision events for video representation and reasoning, 2020.

Zaheer, M., Kottur, S., Ravanbakhsh, S., Póczos, B., Salakhutdinov, R., and Smola, A. Deep sets. In *NIPS*, 2017.

Zintgraf, L. M., Schulze, S., Lu, C., Feng, L., Igl, M., Shiarlis, K., Gal, Y., Hofmann, K., and Whiteson, S. Varibad: Variational bayes-adaptive deep rl via meta-learning. *Journal of Machine Learning Research*, 22: 289:1–289:39, 2021.

Zuccaro, G., Gregorio, D. D., and Leone, M. F. Theoretical model for cascading effects analyses. *International Journal of Disaster Risk Reduction*, 2018.

A. Additional results

Here we describe additional results and provide further discussion.

	UNCONSTRAINED	BOTTLENECK	COUNT	B & C
ROSETTE (OURS)	76.5 ± 0.8%	68.5 ± 1.0%	60.8 ± 0.7%	49.5 ± 0.5%
-COUNT	75.8 ± 0.9%	68.4 ± 0.8%	6.1 ± 0.6%	17.1 ± 0.5%
-BOTTLENECK	76.4 ± 0.9%	21.5 ± 1.1%	61.1 ± 1.2%	34.1 ± 0.7%
-COUNT -BOTTLENECK	76.6 ± 0.8%	21.4 ± 1.1%	6.1 ± 0.5%	4.2 ± 0.3%
-FULL	60.8 ± 0.5%	32.7 ± 0.9%	11.7 ± 0.5%	6.6 ± 0.1%
SEQUENTIAL	77.9 ± 0.4%	66.9 ± 1.3%	46.3 ± 1.3%	36.5 ± 1.3%

Table 4. **Ablation study.** In red, results that perform much worse than ROSETTE.

A.1. Baseline results discussion

(Qi et al., 2021) baseline: We believe that the (Qi et al., 2021) baseline fails for three main reasons: (1) The baseline does not use an event-based representation. (2) It employs a classifier that is trained to provide an all-or-none signal, rather than guiding the search. The ablation study (Table 1, right) demonstrates the importance of guiding the search (compare “Ours” 59.7% vs “All-or-None” 33.5%) (3) The baseline architecture cannot reason over the temporal DAG structure of a cascade, as our GNN can. The importance of capturing the DAG structure is demonstrated when comparing “Our” (60.8%) to the SEQUENTIAL baseline (52.4%) (Table 1, left)

Existing Planners: We wish to provide further insight into why it is challenging to apply existing planners to this setup. The main challenge is that the optimization objective is given in semantic terms about the end goal. To apply a Cross-Entropy-Method (CEM) planner, we derive a corresponding objective function by training a classifier that checks if the goal was achieved for a given scene and plan. Specifically, we used the existing SoTA PHYRE classifier (Qi et al., 2021). A main drawback is that classifiers provide an “all or none” signal, hence fail in guiding the planner through optimization. Conversely, our approach provides a score (Eq. 1) that monotonically increases through the tree, and it is constructed to assist the search.

B. Qualitative examples

Here we provide links to qualitative examples that we uploaded to YouTube. They are best viewed in $\times 0.25$ slow motion. The YouTube account we use is anonymous.

For each episode, we show a side-to-side video of the observed cascade, the ROSETTE successful case, and ROSETTE-max-l failure case. The instruction is displayed on top of each video.

- *Push: cyan ball, Target: blue hits red, Bottleneck: cyan hits bottom wall, Chain Count: 6*
In this example, ROSETTE semantically follows the first 10 collisions (in chronological order) as in the observed cascade. It then diverges from the observed cascade, making the blue hit the red. The cyan pivot comes into play already on the 1st collision, and the agent adjusts its velocity such that it shall yield the goal. The ROSETTE-max-l baseline, hits the target, however it fails with the count constraint. The bottleneck collision occurs, but not on the chain from the pivot to the target. See the complete video here: <https://youtu.be/RCKFBRrCRw0>
- *Push: cyan ball, Target: green hits red, Bottleneck: purple hits red, Chain Count: 4*
In this example, ROSETTE semantically follows the first 5 collisions (in chronological order) as in the observed cascade. The cyan pivot comes into play on the 3rd collision. It then diverges from the observed cascade, and follows another chain of events, making the purple hit the red, and concluding with the target hit within 4 collisions in the chain that started at the cyan ball. This task is too hard for the ROSETTE-max-l baseline, as it completely fails to satisfy the instruction. See the complete video here: https://youtu.be/4s9MmY2J_I
- *Push: green ball, Target: green hits cyan, Bottleneck: green hits purple, Chain Count: 5*
In this example, ROSETTE semantically follows the first 6 collisions (in chronological order) as in the observed cascade. It then diverges from the observed cascade, making the green hit the purple, fulfilling the bottleneck constraint. The cyan pivot comes into play only on the 6th collision, and the agent adjusts its velocity such that both the target and the

count constraint will be satisfied. The ROSETTE-max-1 baseline, hits the bottleneck, however it fails to hit the target. See the complete video here: https://youtu.be/iMedd_7YndQ

- *Push: yellow ball, Target: cyan hits red, Bottleneck: purple hits red, Chain Count: -*
In this example, ROSETTE semantically follows the first 5 collisions (in chronological order) as in the observed cascade. The yellow pivot comes into play only on the 5th collision, and the agent adjusts its velocity to satisfy the bottleneck constraint and the target. The ROSETTE-max-1 baseline, completely fails in this task. See the complete video here: <https://youtu.be/QLMTD6R2Z54>
- *Push: red ball, Target: blue hits red, Bottleneck: red hits bottom wall, Chain Count: -*
In this example, ROSETTE semantically follows the first 4 collisions (in chronological order) as in the observed cascade. The red pivot comes into play already on the 2nd collision, and the agent adjusts its velocity to satisfy the bottleneck constraint and the target. The ROSETTE-max-1 baseline, satisfy the bottleneck but does not satisfy the target. See the complete video here: <https://youtu.be/vT1ivd1ECJs>
- *Push: yellow ball, Target: blue hits purple, Bottleneck: blue hits right wall, Chain Count: -*
In this example, ROSETTE semantically follows only the first 2 collisions (in chronological order) as in the observed cascade. The red pivot comes into play on the 3rd collision, and the agent adjusts its velocity to satisfy the bottleneck constraint and the target. The ROSETTE-max-1 baseline, completely fails in this task. See the complete video here: <https://youtu.be/rgzWBfx-LqY>

Importantly, these examples demonstrate the usefulness of the observed cascade for tree search. ROSETTE followed the observed cascade along the part of the path that was useful to satisfy the instruction. It diverged from the path when necessary, and found a solution when long cascades were essential, while ROSETTE-max-1 struggled.

Finally, we note that this observation is also quantitatively supported: As we show in Figure 4 and Figure A.3. When conditioning the Tree Success rate on producing long cascades, with *Chain count* constraint values greater or equal to 5, ROSETTE performs at $34.8 \pm 0.8\%$, while ROSETTE-max-1 performs at $31.3 \pm 1.1\%$, showing $\sim 11.1\%$ improvement. For *Chain count* values smaller than 5, they are statistically equivalent $75.1 \pm 0.4\%$ and $75.4 \pm 0.4\%$.

C. User study

We conducted a user study with Amazon Mechanical Turk (AMT) using 30 test episodes. We designed a game where a player (rater) is given a video of the observed cascade and is asked to select one of 44 combinations of orientations (11) and relative speeds (4) (magnitude of velocity). One combination of orientation and speed was aligned with the ground-truth solution, and the rest were spaced in relation to that solution. In an offline stage, we tested which of the *other* orientations and speeds satisfy the goal and included those as valid solutions. We allowed the players to freely replay the observed video. We paid 1\$ per game.

Figure A.1 shows one test episode. The upper panel provides an instruction that states the goal of that specific episode. On the left, we provide a set of simple guidelines. The center panel provides the observed (failed) video. The right panel shows the initial frame, overlaid with the set of possible orientations and a set of HTML radio buttons to select the orientation and speed. The upper tab provides a set of four examples with solutions and explanations. Those examples are given in Figure A.2.

To maintain the quality of the queries, we only picked users with AMT “masters” qualification, demonstrating a high degree of approval rate over a wide range of tasks. Furthermore, we also executed a qualification test with a few curated episodes that are very simple. To qualify users, we made sure they do not randomly pick an answer by only qualifying users who completed 5 episodes and had a single error at most. Additionally, we deleted queries from one qualified user, who submitted answers at a rate of 3-4 episodes per minute, as we qualitatively observed that it should take 1-3 minutes to complete an episode.

Qualified users received a bonus of 0.5\$, accompanied with the following message:

Thank you for doing the qualification batch for our colliding balls game.
Our full study is now online. You can start doing it. Please remember to **PLAY THE VIDEO** and use it to decide about your answer. And also, take another look at the examples, as they can provide more intuition about the task.

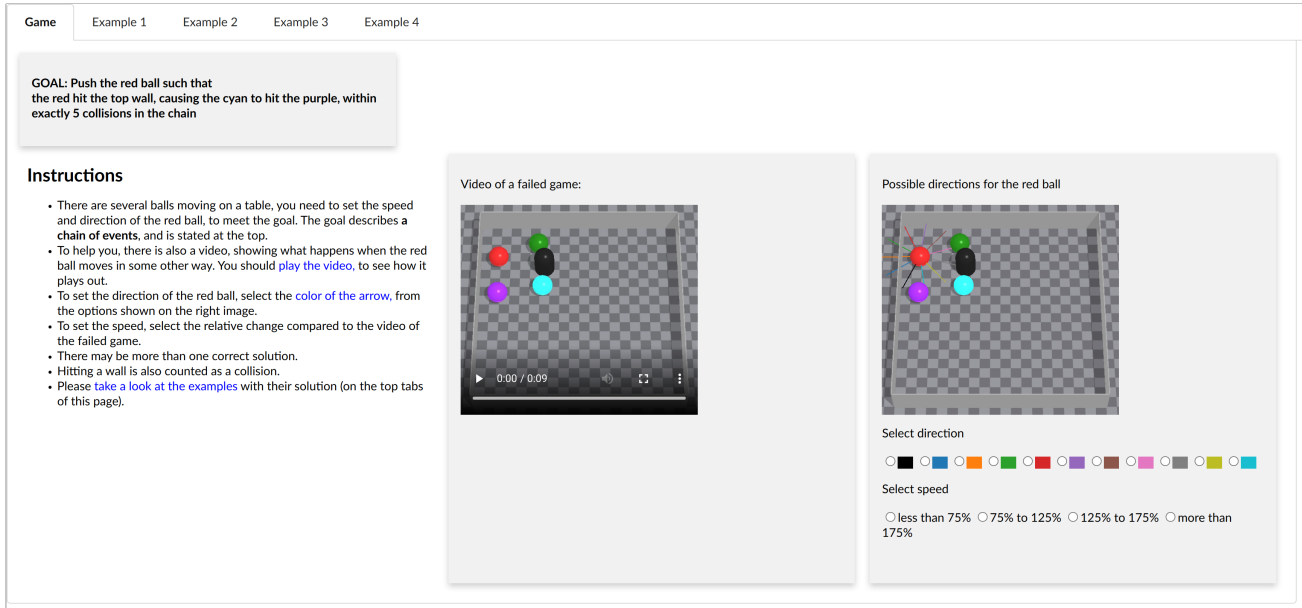


Figure A.1. One test episode of the user study. See Section C for details.

11 players have passed our qualification tests, playing 25 episodes on average. Table 5 compares the human success rate with ROSETTE and a Random baseline. Showing Average, Median and Best statistics. For the Median and Best statistics, we only included users who played a minimum number of 20 episodes (8 of 11 users).

	Average	Median	Best
Random	17.6 ± 1.1%		
Humans	23.9 ± 2.6%	25%	41.4%
ROSETTE	43.3 ± 1.3%	43.3%	46.7%

Table 5. Success rate statistics for the user study. ± error denotes the standard error of the mean (S.E.M) across the samples.

D. Additional experimental details

D.1. Hyperparameter tuning

We train the model and baselines for 15 epochs. Batch size was set to 8192 to maximize the GPU memory usage. We use the PyTorch’ default learning rate for Adam (Kingma & Ba, 2015) (0.001). For inference, we set $N_{observed}$ to 9, the maximal tree depth to 30, we sample 10^6 initial states and expand 80 nodes per episode which takes ~ 13 seconds. The GNN uses 5 layers, with a hidden state dimension of 128. Hyper parameters were tuned one at a time, during an early experiment on a validation set.

D.2. Random Baseline

We sample an intervention at random from an estimated distribution of ground-truth interventions. The distribution is estimated by calculating a 2D-histogram with 30×30 , and approximating the distribution within each bin to be uniform.

D.3. Deepset regression Baseline




Overview: For the Deepset regression baseline, we embed the instruction and the initial world state to predict a continuous intervention. We use the permutation-invariant “Deep Sets” architecture (Zaheer et al., 2017), and use an L_2 loss with respect to ground-truth interventions in the “counterfactual” training samples.


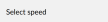
Learning to Initiate and Reason in Event-Driven Cascading Processes

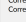
Game Example 1 Example 2 Example 3 Example 4

In this example we set the direction of the cyan ball toward the top left, with a low speed, so it will hit the green ball once it arrives there.

GOAL: Push the cyan ball such that the cyan hit the green

Video of a failed game:  Possible directions for the cyan ball:  A solution: 




Select direction: 
 Select speed: 
 less than 75%, 75% to 125%, 125% to 175%, more than 175%


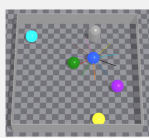
Correct Direction: 
 Correct Speed: less than 75%

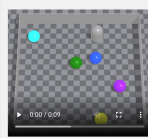
Game Example 1 Example 2 Example 3 Example 4

In this example we set the direction of the yellow ball toward the left wall, with a high speed, so it will bounce back from the wall and hit the cyan ball.

GOAL: Push the yellow ball such that the yellow hit the left wall, causing the yellow to hit the cyan

Video of a failed game:  Possible directions for the yellow ball:  A solution: 




Select direction: 
 Select speed: 
 less than 75%, 75% to 125%, 125% to 175%, more than 175%


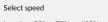
Correct Direction: 
 Correct Speed: more than 175%


Game Example 1 Example 2 Example 3 Example 4

In this example we set the direction of the purple ball, with a relatively higher speed, to hit the cyan and in turn hit the red ball. In total there are two collisions in this chain of events: (1) purple hits cyan, (2) cyan hits red.

GOAL: Push the purple ball such that the cyan hit the red, within exactly 2 collisions in the chain

Video of a failed game:  Possible directions for the purple ball:  A solution: 

Select direction: 
 Select speed: 
 less than 75%, 75% to 125%, 125% to 175%, more than 175%


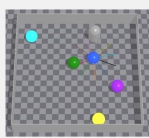
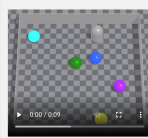
Correct Direction: 
 Correct Speed: 125% to 175%


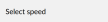
Game Example 1 Example 2 Example 3 Example 4

In this example we set the tune direction of the blue ball, to hit with the green and in turn hit the right wall, bounce back and hit the green again. In total there are three collisions in this chain of events: (1) blue hits green, (2) blue hits right wall, (3) blue hits green.

Note that the video provided a hint for how to solve this game.

GOAL: Push the blue ball such that the blue hit the green, causing the blue to hit the green again, within exactly 3 collisions in the chain

Video of a failed game:  Possible directions for the blue ball:  A solution: 

Select direction: 
 Select speed: 
 less than 75%, 75% to 125%, 125% to 175%, more than 175%

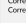
Correct Direction: 
 Correct Speed: 75% to 125%

Figure A.2. Examples provided in the user study. See Section C for details.

The input to the Deepset architecture (Zaheer et al., 2017) is a set of feature vectors. Each feature vector corresponds to a dynamic or static object in the scene. The output is a vector $\in \mathbb{R}^2$, for predicting the controlled velocity of the pivot object.

Feature representation: Each feature vector in the set is represented by a concatenation of the following fields $[obj_feat(o), instruction_emb, position, velocity]$, where $obj_feat(o)$ is defined by Eq. (4), $instruction_emb$ is defined by Eq. (7), $position, velocity$ are the initial position and velocity of the object, as given by the observed cascade.

Labels and loss: For ground-truth labels, we use the ground-truth velocity of the solution. We use a L_2 loss comparing the ground-truth labels with the output of the Deepset architecture.

D.4. (Qi et al., 2021) Baseline

Overview: **Qi2021** is the state-of-the-art approach for solving PHYRE. It uses a learned forward model, a learned goal-satisfaction classifier, and exhaustive search. For a fair comparison with our analytic event-driven forward model, we replace their learned forward model by a full simulator (Makoviychuk et al., 2021).

Therefore, for the goal-satisfaction classifier, in each frame, we replace the set of input feature vectors coming from the region-proposal-interaction-network (RPIN) of (Qi et al., 2021) by a set of feature vectors corresponding to each object in the scene, and its kinematic state as given by the simulator. To condition the classifier on the goal, we concatenate the instruction representation to each feature vector.

Feature representation: Each feature vector of an object in a frame, is represented by a concatenation of the following fields $[obj_feat(o), instruction_emb, position, velocity, time]$, where $obj_feat(o)$ is defined by Eq. (4), $instruction_emb$ is defined by Eq. (7), $position, velocity, time$ are the respective readings from the simulator in the frame.

Positive and Negative examples: For training the goal-satisfaction classifier with positive examples, we use the simulation of the solution cascade. For negative examples, we use the simulation of the observed cascade.

Classifier Architecture: We use the classifier architecture of (Qi et al., 2021), as provided in their public implementation, with the following adaptations: (1) We replace the RPIN representation by the simulator-driven representation described above. (2) We allow replacing the last fully connected layer by a multi-layer-perceptron (MLP) (3) We allowed more than four equally spaced input frames.

Simulator configuration: The RPIN forward model is a fixed timestamp model, working at 1 frame-per-second. In the full simulator we used (Makoviychuk et al., 2021), we observed that it does not perform well in such a coarse-grained resolution, making objects to sometimes go through the walls. Therefore, we increased the simulator resolution to 10 frames-per-second.

Hyperparam search: We searched for the best hyper-parameters configuration that minimizes the validation loss over the following ranges: *Number of MLP hidden-layers* $\in [0, 1, \dots, 6]$, *Number of input frames* $\in [4, 6, 10, 20]$, *batch-size* $\in [128, 256]$. *Number of training epoch* was set according to early stopping on the validation set.

Finally, we used the following hyper-parameters to evaluate the model performance on the test set: *Number of MLP hidden-layers* = 2, *Number of input frames* = 4 (as in (Qi et al., 2021) paper), *batch-size*=128, *Number of training epoch* = 17.

Evaluation: For evaluation, we randomly selected a subset of 208 episodes (10% of the test subset), because inference for a single episodes took ~ 5.5 minutes.

D.5. Cross entropy Baseline

Overview: The cross entropy method is a black box optimizer for solving optimization problems. We used (Qi et al., 2021) baseline’s classifier as our objective function. At each step, we sampled 100 points and updated the sampling distribution based on their score. We have repeated this process for 100 iterations, and chosen the highest scored intervention for evaluation. Our code is based on a standard implementation Greenberg et al. (2022) of the cross entropy method.

For evaluation, we randomly selected a subset of 208 episodes (10% of the test subset), because inference for a single episodes took ~ 4 minutes.

D.6. Sequential Baseline

We used the validation set to select the number of layers for this baseline, $\in [5, 10, 20, 30]$. There wasn’t any significant difference when using 5 or 10 layers, and the success rate degraded for 20 or 30 layers. Therefore, we used 5 layers for evaluating performance on the test set.

D.7. Instruction ablation Baselines

We report the “count” and “bottleneck” ablations by zeroing their respective features in the instruction and using the same model weights that were used to report the performance of the ROSETTE model. We did not retrain the model for these cases because the ROSETTE model was trained to handle these cases, as is evident by the “Unconstrained” metric.

For ablating the “full” instruction, we retrained the model, while completely zeroing the representation vector of the input instruction.

E. Implementation details of the model of the score function

We use a Graph Neural Network (GNN) to parameterize our score function. We represent the graph as a tuple (A, X, E, z) where $A \in \{0, 1\}^{n \times n}$ is the graph adjacency matrix, $Y \in \mathbb{R}^{n \times d}$ is a node feature matrix, $E \in \mathbb{R}^{m \times d'}$ is an edge feature matrix, and $z \in \mathbb{R}^{d''}$ is a global graph feature. we chose to use a popular message passing GNN model (Battaglia et al., 2018) that maintains learnable node, edge and global graph representations.

Architecture The model is composed of several message passing layers, $L^k \circ \dots \circ L^1$ where each L^i updates all representations, i.e.:

$$X^{i+1}, E^{i+1}, z^{i+1} = L^i(A, X^i, E^i, z^i; \theta^i),$$

Each layer L_i updates the features sequentially: the node and edge features are updated by aggregating local information, while the global feature is updated by aggregating over the whole graph. We denote the parameters of the MLPs that are used in a layer L_i as θ_i , and note that these are the only learnable parameters in the model. At the last layer $i = k$ we use a single dimension for the global feature, i.e., $d' = 1$, which is then used as the score of the event node.

Feature representation We describe next the feature representation of the inputs to the node feature matrix Y , the edge feature matrix E , and the global graph feature z .

We start by describing a feature representation of any of the dynamic and static objects in the scene: An object o feature representation, noted by $obj_feat(o)$, is a concatenation of the following fields

$$obj_feat(o) = [one_hot(o), is_stationary, is_active, instruct_inner_prod, bottleneck_ind, count, count_ind], \quad (4)$$

where $one_hot(o)$ is a one-hot vector $\in \mathbb{R}^{12}$, as represented by the instruction; $is_stationary$ indicates whether the object is stationary; is_active means that in the context of a current collision, the object dynamics were coming from a collision chain that included the pivot; $instruct_inner_prod$ is the results of an inner product of $one_hot(o)$ with each of the 5 object representations at the instruction embedding (Section H.3). Finally, $bottleneck_ind, count, count_ind$ are copied from the instruction embedding.

The graph node and edge features are derived from the DAG representation (Figure 3). Each row of the node feature matrix Y concatenates the two objects that participate at a collision $[obj_feat(obj_a), obj_feat(obj_b)]$. Each row at the edge feature matrix E represents $obj_feat(o)$ of the object on that edge.

Last, the global feature z is a copy of the instruction embedding Eq. (7).

Training data For calculating the training labels of the score function, we traverse the semantic tree along the ground-truth sequence of the solution cascade and collect the *positive* labels using Eq. (2). If the event tree cannot reproduce the solution

sequence of a sample (due to errors accumulated by the event-driven forward model), then Eq. (2) cannot be calculated, and we drop that sample from the training set. We collect *negative* examples (with $V = 0$) by (1) taking the child nodes that diverge from the path to the ground-truth solution. (2) Traverse a random path along the tree with the same length as the ground truth sequence, and set the score of all the nodes along that path to 0. Note that setting the scores of every node along these paths to $V = 0$ is a heuristic and may introduce some label noise with respect to negative examples. Additional research may be required to analyze the label-noise consequences and address it.

F. Counterfactual update for the score function

In this section, we derive the expression of the score function update according to the observed cascade (Eq. (3)). We start the derivation by repeating the preliminary derivation steps introduced in the main text in more detail.

During inference, we observe a cascade that does not satisfy the instruction, and are asked to retrospectively suggest a better solution. How can the information can be used to find a better solution? The probabilistic score function allows us to formalize this problem in a Bayesian setting. We treat the model predictions as a *prior* for the true score, and the information about the observed cascade as *evidence*. We then ask how to update the score function given the observed evidence. Formally, we condition Eq. (1) by the evidence, $V(u|S_{u^{obs}}$ doesn't satisfy g).

We denote the set of interventions that satisfy the instruction g as $\mathcal{G}_g \subset \mathcal{Y}$, and the evidence by E . Note that an equivalent definition for the *unconditioned* score function $V(\cdot)$ is

$$\begin{aligned} V(u) &= \Pr(Q(y) \text{ satisfies } g | y \in Y_u, g) \\ &= \Pr(y \in \mathcal{G}_g | y \sim U(Y_u)) \end{aligned}$$

Our evidence is that for a particular $\tilde{y} \in Y_{obs}$, we have $\tilde{y} \notin \mathcal{G}_g$. Now, by definition, every $y, y' \in Y_{obs}$ share the same observed cascade $S_{u^{obs}}$. Therefore, the evidence E can be equally formulated as $y' \notin \mathcal{G}_g$ for any y' sampled uniformly from $Y_{u^{obs}}$, $y' \sim U(Y_{u^{obs}})$. For brevity, we set $Y_{obs} = Y_{u^{obs}}$.

The *conditioned* score function is then,

$$\Pr(y \in \mathcal{G}_g | y \sim U(Y_u), E)$$

We use the law of total probability and write,

$$\begin{aligned} &\Pr(y \in \mathcal{G}_g | y \sim U(Y_u), E) \\ &= \Pr(y \in \mathcal{G}_g | y \sim U(Y_u), E, y \in Y_{obs}) \Pr(y \in Y_{obs} | y \sim U(Y_u), E) \\ &\quad + \Pr(y \in \mathcal{G}_g | y \sim U(Y_u), E, y \in Y_{obs}^c) \Pr(y \in Y_{obs}^c | y \sim U(Y_u), E) \\ &= \Pr(y \in \mathcal{G}_g | y \sim U(Y_u \cap Y_{obs}), E) \Pr(y \in Y_{obs} | y \sim U(Y_u), E) \\ &\quad + \Pr(y \in \mathcal{G}_g | y \sim U(Y_u \cap Y_{obs}^c), E) \Pr(y \in Y_{obs}^c | y \sim U(Y_u), E) \end{aligned}$$

Furthermore,

$$\begin{aligned} \Pr(y \in Y_{obs} | y \sim U(Y_u), E) &= \Pr(y \in Y_{obs} | y \sim U(Y_u)) \\ \Pr(y \in Y_{obs}^c | y \sim U(Y_u), E) &= \Pr(y \in Y_{obs}^c | y \sim U(Y_u)) \end{aligned}$$

As the conditioned event $y \in Y_{obs}$ is independent of E .

The relations between node U^{obs} and u can be one of the three: a) the observed node is a descendant of u (and therefore $Y_u \cap Y_{obs} = Y_u$) b) u and the observed node belong to different branches, and therefore $Y_u \cap Y_{obs} = \emptyset$, or c) u is a descendant of the observed node (and therefore $Y_u \cap Y_{obs} = Y_{obs}$). However, u^{obs} represents a complete cascade rather than a partial sequence, and therefore the observed node does have any children, and we can ignore c).

Let us consider each case separately.

u and the observed node are along different paths. In this case,

$$\begin{aligned} Y_u \cap Y_{obs} &= \emptyset \\ Y_u \cap Y_{obs}^c &= Y_u \\ \Pr(y \in Y_{obs}^c | y \sim U(Y_u)) &= 1 \\ \Pr(y \in Y_{obs} | y \sim U(Y_u)) &= 0, \end{aligned}$$

and we're left to evaluate $\Pr(y \in \mathcal{G}_g | y \sim U(Y_u), E)$. Since the evidence in this case provides information about a set that y is not conditioned on, it is independent of y , and therefore we conclude with,

$$\Pr(y \in \mathcal{G}_g | y \sim U(Y_u), E) = \Pr(y \in \mathcal{G}_g | y \sim U(Y_u)) = V(u)$$

u is a descendant of the observed node. Here,

$$\begin{aligned} Y_u \cap Y_{obs} &= Y_{obs} \\ \Pr(y \in Y_{obs} | y \sim U(Y_u)) &= fr(y_{obs}, y_u) \end{aligned}$$

In this case,

$$\begin{aligned} &\Pr(y \in \mathcal{G}_g | y \sim U(Y_u), E) \\ &= \Pr(y \in \mathcal{G}_g | y \sim U(Y_u \cap Y_{obs}), E) fr(y_{obs}, y_u) \\ &+ \Pr(y \in \mathcal{G}_g | y \sim U(Y_u \cap Y_{obs}^c), E) (1 - fr(y_{obs}, y_u)) \\ &= \Pr(y \in \mathcal{G}_g | y \sim U(Y_{obs}), E) fr(y_{obs}, y_u) \\ &+ \Pr(y \in \mathcal{G}_g | y \sim U(Y_u \cap Y_{obs}^c), E) (1 - fr(y_{obs}, y_u)) \end{aligned} \quad (5)$$

Now,

$$\begin{aligned} &\Pr(y \in \mathcal{G}_g | y \sim U(Y_{obs}), E) \\ &= \Pr(y \in \mathcal{G}_g | y \sim U(Y_{obs}), \{\forall y' \in Y_{obs}, y' \notin \mathcal{G}_g\}) \\ &= 0 \end{aligned}$$

Since the evidence indicates that for every $y' \in Y_{obs}$ the resulting sequence $S_{u_{obs}}$ does not satisfy the goal. Furthermore,

$$\Pr(y \in \mathcal{G}_g | y \sim U(Y_u \cap Y_{obs}^c), E) = \Pr(y \in \mathcal{G}_g | y \sim U(Y_u \cap Y_{obs}^c)) \quad (6)$$

As E does not add information when we sample from $(Y_u \cap Y_{obs}^c)$.

Therefore,

$$\Pr(y \in \mathcal{G}_g | y \sim U(Y_u), E) = \Pr(y \in \mathcal{G}_g | y \sim U(Y_u \cap Y_{obs}^c)) (1 - fr(y_{obs}, y_u))$$

Now

$$\begin{aligned} \Pr(y \in \mathcal{G}_g | y \sim U(Y_u)) &= \Pr(y \in \mathcal{G}_g | y \sim U(Y_u \cap Y_{obs})) fr(y_{obs}, y_u) \\ &+ \Pr(y \in \mathcal{G}_g | y \sim U(Y_u \cap Y_{obs}^c)) (1 - fr(y_{obs}, y_u)) \end{aligned}$$

Namely,

$$V(u) = V(u_{obs}) \cdot fr(y_{obs}, y_u) + \Pr(y \in \mathcal{G}_g | y \sim U(Y_u \cap Y_{obs}^c)) (1 - fr(y_{obs}, y_u))$$

or

$$\Pr(y \in \mathcal{G}_g | y \sim U(Y_u \cap Y_{obs}^c)) = \frac{V(u) - V(u_{obs}) \cdot fr(y_{obs}, y_u)}{1 - fr(y_{obs}, y_u)}.$$

Plugging this back to Eq. 6 we obtain:

$$\Pr(y \in \mathcal{G}_g | y \sim U(Y_{obs}), E) = V(u) - V(u_{obs}) \cdot fr(y_{obs}, y_u)$$

which is our final result.

G. Relation to Causal-Inference

The DAG representation (Section 3.2) is useful for graphically representing one instance of a cascade, but we intentionally avoid naming it a *Causal* DAG, because it can't represent dependencies between events that are not explicitly observed in the video. E.g., in the example $[(A, B), (C, D), (A, E)]$ in Section 3.2, it may be that (A,E) depends on (C,D) because C blocks D from reaching to E before A do. The event tree can simulate this behaviour, while the DAG (C,D) ; (A,B)- \rightarrow (A,E) is unaware of it. From a formal causal inference perspective (Pearl, 2000), our event tree is the part of our approach that can be related to the formal "Structured" Causal Model (SCM). As it is a generative model that reflects the data generation process; it can account for complex dependencies between events; and every edge corresponds to a function, namely, the event-driven forward model.

H. Data generation details

H.1. Video generation details

In this section, we describe the generation process of the dynamical scene. We first create an "unperturbed" video. Then, we perturb the video by modifying the velocity of a specific element, which will be later designated as the pivot. We let the perturbed video roll out, validate that it is indeed semantically different than the unperturbed video, and label it as the "observed" video. The unperturbed video can now be used as reference for our instruction generation process. It is a realization of a specific, complex, semantic chain of events that is both semantically different than the perturbed ("observed") video and is also feasible, e.g, by setting the intervention value as to revert the perturbation. This flow guarantees that we can ask meaningful instructions on the "observed" that are guaranteed to be realizable.

The unperturbed video. We construct the unperturbed video by iteratively adding spheres and collisions in a physical simulator (IsaacGym (Makoviychuk et al., 2021)) increasing the video complexity. We start by placing a sphere in the confined four-walled space and assign it a random velocity.

The dynamics of a sphere moving freely in a confined square area can be expressed analytically. We pick a random time t_1 , hitting velocity, and hitting angle for the first collision. We analytically solve for the initial position and velocity at $t_0 = 0$ that will result in the a collision at t_1 with the specific hitting velocity and angle. We assign these value to a randomly colored sphere.

Due to discrepancies between the simulator dynamics and the kinematic analytic model, we roll out the dynamical system in the simulator, and record the system state immediately after a collision.

We continue adding spheres iteratively. Given a state at t_i , we randomly select a sphere O_i from the existing spheres, collision time t_{i+1} , hitting angle and velocity. We solve analytically and find the initial position and velocity at $t_0 = 0$ that will result in a collision with O_i corresponding parameters. We roll out the dynamical system, and update the velocities and positions records after each collision with the empirical values from the simulator.

Our simple kinematic model assumes the target sphere and the newly added move freely. However, other spheres may cross their trajectories, resulting in an a collision that will distract the spheres from their designated path. However, this simply means that the planned random collision was replaced by a different collision. Since we update our records of the resulting collisions and corresponding output velocities and positions using the simulator, this does not pose any serious limitations.

The observed video. We pick a random sphere from the set of spheres and assign it a different velocity at $t = 0$. We roll out the system in the simulator and log all resulting collisions. We validate that the resulting collision sequence is different than

the unperturbed video collision sequence. We now have two videos that differ only in the initial velocity of a specific sphere, but result in a substantially different semantic chain of events.

H.2. Instruction generation details

We describe the instruction generation process when given an “observed” video, and a “counterfactual” video that displays an alternative cascade of events.

Given a ground-truth video, its sequence of collisions, and a pivot, we randomly sample an instruction: Starting by randomly sampling a target collision from the sequence. And then, we randomly sample up to two constraints that accompany the goal. For constructing the constraints, we first represent the sequence of collisions using a DAG, in a similar fashion as described in Figure 3, then we use standard NetworkX functionality (Hagberg et al., 2008) for graph traversal: (1) We use “dag.ancestors()” to get a list of nodes for the “bottleneck” constraint. (2) We use “all_simple_paths()” to count the nodes in a chain reaction between the pivot and the target collision.

To avoid trivial goals, we drop an instruction if it is fulfilled by the observed video (rather than the “counterfactual” video). We sample up to 5 unique instructions for each scene (~4 on average).

H.3. Instruction feature representation

We assume perfect lexical perception, and provide the agent with the a structured vector representation of each instruction, by concatenating the following fields:

$$\text{instruction_emb} = [\text{target_obj_a}, \text{target_obj_b}, \text{pivot_obj}, \text{bottleneck_obj_a}, \text{bottleneck_obj_b}, \text{bottleneck_ind}, \text{count}, \text{count_ind}], \quad (7)$$

where $\text{target_obj_a}, \text{target_obj_b}$ are the object representations of the target collision. pivot_obj represents the pivot. $\text{bottleneck_obj_a}, \text{bottleneck_obj_b}, \text{bottleneck_ind}$ represent the two “bottleneck” objects and a binary indicator scalar. If an “bottleneck” constraint is not applicable for an instruction, we them all to 0. $\text{count}, \text{count_ind}$ are 2 scalar values: One for the number of collisions of the chain “count” constraint, and another used as a binary indicator for the “count” constraint. Similarly if a “count” constraint is not applicable for an instruction, we set both count and count_ind to 0.

Finally, note that each object is represented by a one-hot vector $\in \mathbb{R}^{12}$, because the environment has 12 types of unique objects: 6 colored balls, 2 static pins, and 4 walls.

H.4. Complex instructions dataset

For the complex instructions dataset, we add a third object centric constraint that counts the number of interactions a specific object makes on the paths from the pivot to the target collision. It resembles constraining the amount of resources available per instance on a logistic chain. With an additional constraint we can test our approach on a more challenging task that has a large variety of instructions that have 2 or more constraints. We split the evaluation set to “Hard” instructions that have 2 or more constraints, and “Easy” instruction with 0-1 constraints. We generated instructions for the same scenes as in the main dataset, which yields ~4.5 instructions per scene. The test set consists of 2190 episodes, where 54% are “Hard” instructions.

I. The forward model

In our physical setup, the dynamics are prescribed by the position and velocity $c_i^j = (\text{pos}_i^j, \text{vel}_i^j), j = 1 \dots n$ of each of n objects in the environment. The world state w_i^u of a node u is then a tuple

$$w_i^u = (c_i^1, c_i^2, \dots, c_i^n, t_i), \quad (8)$$

where for the root node $t_i = 0$ for all x_i .

The forward module takes as input a world state w_i it outputs the next semantic event (s'), and a state $f(w_i) = w'_i = (c_i^1, c_i^2, \dots, c_i^n, t'_i)$ immediately after the predicted semantic event at t'_i . The section is divided into three parts. First, we describe the analytical equations that control if two objects will collide. Then we show how can leverage the analytic model to efficiently branch out from a node in the event tree. Finally, we fill in the missing details and present the full forward model.

The collision detector. Assume two spheres $i = \alpha, \beta$ moving freely on a plane with an initial velocity of \mathbf{v}_i and position \mathbf{r}_i at $t = 0$. Each sphere has a radius of l_i . If the two spheres collide, then, at the moment of collision, the spheres intersect at a single point. We can use a simple geometric calculation to find their *planar* distance. The distance between the center of spheres is $l_\alpha + l_\beta$, while the vertical distance between the two centers is $|l_\alpha - l_\beta|$. The resulting planar distance is then:

$$d = \sqrt{(l_\alpha + l_\beta)^2 - (l_\alpha - l_\beta)^2} = 2\sqrt{l_\alpha l_\beta}. \quad (9)$$

Therefore, in order to check if the spheres collide, we can check if the planar distance between the two spheres is ever equal to d ,

$$\|\mathbf{r}(t)\|^2 = \|\mathbf{r}_\alpha + \mathbf{v}_\alpha \cdot t - \mathbf{r}_\beta - \mathbf{v}_\beta \cdot t\|^2 = d^2 \quad (10)$$

This is a quadratic equation in t , which we can solve for analytically. If the discriminant is non-negative, the collision time corresponds to the smaller root. The spheres' velocities immediately after the collision are given by:

$$\mathbf{v}'_1 = \mathbf{v}_1 - \frac{2m_2}{m_1 + m_2} \frac{\langle \mathbf{v}_1 - \mathbf{v}_2, \mathbf{y}_1 - \mathbf{y}_2 \rangle}{\|\mathbf{y}_1 - \mathbf{y}_2\|^2} \cdot (\mathbf{y}_1 - \mathbf{y}_2) \quad (11)$$

$$\mathbf{v}'_2 = \mathbf{v}_2 - \frac{2m_1}{m_1 + m_2} \frac{\langle \mathbf{v}_1 - \mathbf{v}_2, \mathbf{y}_1 - \mathbf{y}_2 \rangle}{\|\mathbf{y}_1 - \mathbf{y}_2\|^2} \cdot (\mathbf{y}_2 - \mathbf{y}_1) \quad (12)$$

Likewise, it is trivial to obtain an analytical expression for the collision time and output velocity of a collision between a freely moving sphere and each of the static walls bounding the spheres (should the collision occur). The sphere's velocity in the direction orthogonal to the walls flips, while the parallel velocity remains the same.

Parallelizing collision detection. The collision detector provides an analytic condition that validates whether a specific collision occurs.

$$(\Delta \mathbf{r} \cdot \Delta \mathbf{v})^2 - 4(\|\Delta \mathbf{r}\|^2 - d^2)\|\Delta \mathbf{v}\|^2 > 0 \quad (13)$$

Eqs. 9-13 can be solved in parallel for multiple tuples of $(\mathbf{r}_1, \mathbf{v}_1, \mathbf{r}_2, \mathbf{v}_2)$ on a GPU using packages such as PyTorch. Given an intervention set of Y_u , and a corresponding world-state set W_u , we iterate over all possible collisions $S_{ij} = (O_i, O_j)$. For each collision between object i and j we can apply our collision detector by extracting the corresponding coordinates c_w^i, c_w^j, t_w from $w \in W_u$ (Eq 8). We can do in parallel for all world states $w \in W_u$. If a collision is predicted, we construct a new node child u' of u . We associate with it the interventions for which the collision detector returned a non-null time for the collision, $Y'_{u'}$, the corresponding set of post-collision world state $W'_{u'}$, and the event sequence $S'_{u'} = \text{concat}(S_u, (O_i, O_j))$

The complexity is quadratic in the number of object rather than linear in the number of interventions. This allows us to apply our algorithm with a high number of interventions, and therefore enable us to consider delicate sequences of collision that would require refined "trick shots".

This approach considers every two objects O_i, O_j as moving freely. However, another object in the environment, e.g. O_k , may interact with O_i (without loss of generality) before the collision. This necessarily means that the collision time t_{ik} precedes t_{ij} . In order to account for this, we hold an additional structure that maintains the minimal collision time for every $w \in W_u$. We update it as we iterate over all possible collisions. Then, we associate each $w \in W_u$ and its corresponding $y \in Y_u$ to the event node corresponding to the collision with the earliest collision time.

J. Additional setups

Here, we present examples for additional setups for which our formalism can be applied.

J.1. Logistics

While logistics is a complex field, we describe a simple model that captures the essential components of a logistics problem.

Consider a large logistics enterprise that needs to coordinate shipping from multiple locations. The enterprise has multiple carriers (e.g, trucks or airplanes) $v_i, i = 1..m$ and routes them between logistic centers at $r_j, j = 1..n$.

A plan is a schedule for each carrier τ_j , where a schedule τ_j is a sequence of arrivals and departures between various logistic centers,

$$\tau_j = \{(r_j^0, t_{in}^0, t_{out}^0), (r_j^1, t_{in}^1, t_{out}^1), \dots\}$$

Not all plans are *feasible*. Each carrier can travel at a range of velocities, resulting in a range of arrival times to the possible destinations. Carriers can exchange cargo is they are present at the same logistic center.

Now, assume a logistic center is suddenly shut down. Rescheduling all carriers is unfeasible, as some may be already committed to a route, or may not be easily diverted (e.g., are airborne). Furthermore, recomputing a new plan for the complete enterprise might be computationally heavy. Finally, it seems reasonable that re-planning of only the routes of carriers that were suppose to arrive to the closed logistic center may be enough. We denote those k carriers as the *rescheduled carriers*. Note that while only some of routes may be re-planned, other carriers might be affected as well due to a cascade of delays or even cargo exchange cancellations.

Such re-planning may be constrained by semantic instruction. For example: "Carrier X should only make two deliveries", "Carrier Y should meet carrier Z before meeting Carrier W", etc. .

We now cast this problem into our general framework, described in Section 3. An event is the arrival or departure of a carrier to a logistic center. Each intervention $y \in \mathcal{Y}$ is a set of plans the rescheduled carriers,

$$y = (\tau_0, \tau_1, \dots, \tau_k).$$

A world state w_j is the position of the k carriers at different time $((p_j^0, t_j^0), \dots, (p_j^k, t_j^k))$ The forward model takes as input a world state and outputs all world state that obey the following two rules: 1) At least one carrier moved to a different logistic center. 2) The transition of carriers follow physical constraints. If carrier i can move at velocity range $[v_{min}^i, v_{max}^i]$ and it moves between two logistics centers r_a and r_b , then the transition time must be in

$$\left[\frac{\|r_a - r_b\|}{v_{max}^i}, \frac{\|r_a - r_b\|}{v_{min}^i} \right]. \quad (14)$$

For simplicity, we assume that there is no cargo limit.

The expressions for the induced probability, Eqs. 2-3, remains the same.

J.2. Failure cascades in power grids

Cascading failures in power grid may cause large blackout with substantial economical damage (Schäfer et al., 2018). Cascading Power failures may be induced due to random fluctuations and can develop on orders of seconds. Human operators or complex control mechanism may not be able react in time. The transmission system operator may use an event-driven forward model to find fast automated reactions for unseen dynamical configurations to avoid cascading failures.

Here, semantic events are failures of nodes (nodes; e.g., transformers, power generators, etc.) or power lines (edges). Power flow follows a known set of ODE for a given grid (eqs 14-15 in (Schäfer et al., 2018)):

$$\frac{d}{dt}\theta_i = \omega_i, \quad (15)$$

$$I_i \frac{d}{dt}\omega_i = P_i - \gamma_i \omega_i + \sum_{j=1}^N K_{ij} \sin(\theta_j - \theta_i), \quad (16)$$

where, θ_i, ω_i are the dynamical variable at node i , P_i is the power input (or output) at node i , and K_{ij} is a weighted adjacency matrix representing the grid connectivity. If at some point in time the flow $F_{i,j}$ exceeds the powerline capacity $\alpha k_{ij}, \alpha \in [0, 1]$ (eqs 1-2), the line fails. This condition can be formally written as

$$F_{ij}(t) = K_{ij} \sin(\theta_j(t) - \theta_i(t)) > \alpha K_{ij}.$$

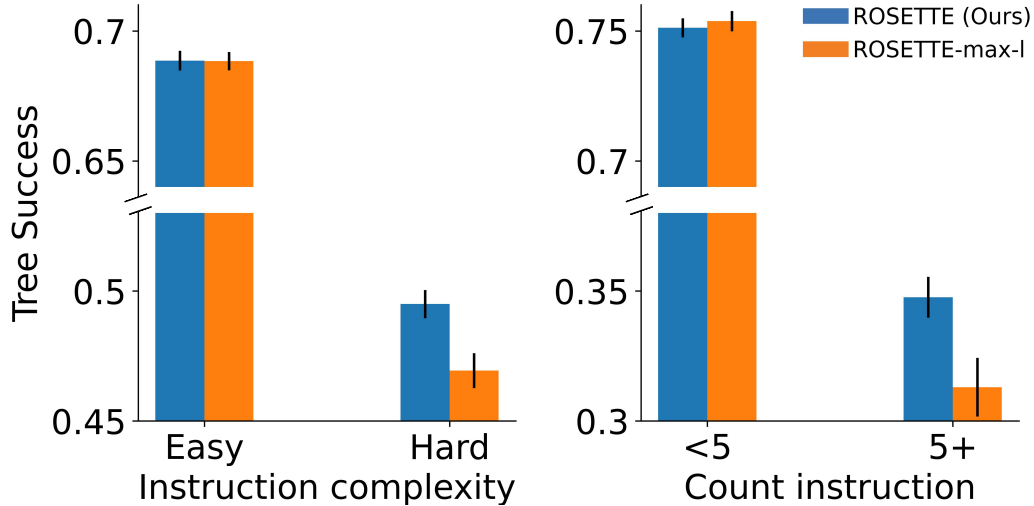


Figure A.3. Comparing “Counterfactual” search (ROSETTE) with “Maximum likelihood” search (ROSETTE-max-l) for 2 levels of instruction complexity (“Hard”: 2 or more constraints) and for two levels of “count” instructions (“5+”: 5 or more). **Here we use the main dataset.** Using the observed cascade, ROSETTE performs better in complex scenarios.

If the line fails, the dynamics are governed by a new effective coupling matrix $K_{i,j}$, and the dynamics in Eqs. 15-16 changes accordingly.

A failure of a node may induce outage to some region. The transmission system operator (TSO) might define goals such as “no more than three failures”, “the maximal number of affected people should be less than n ”, “these highly important nodes should not fail” etc.

J.3. Evolution of natural disasters

Finally, another use case is the evolution of natural disasters. (Zuccaro et al., 2018) provides a full description of an event tree. It models transitions between events like a “seismic shock” which can lead to “landslide” and result with “traffic accident”, and how taking preventive measures like “evacuate population” can influence the total damage caused by the crisis.

K. Complex scenario conditioning for the main dataset

In Figure A.3 we provide the results for complex scenario conditioning for the main dataset (with two type of constraints). The results demonstrate a similar trend as in the complex instruction dataset in Figure 4.

L. An alternative Markov Reward Process Formalism

To describe our approach in Markov Reward Process (MRP) terms, one should first find the analogue of MRP states in our system. A straightforward approach would be to treat each physical state as a state of the MRP. Yet, in our approach, an event tree node represents a set of physical states that have a common sequence of semantic events preceding them. We developed a representation, the event-tree, which aggregates physical states into semantic events, corresponding to MRP states.

Next, one should find parallels between the MRP reward and value function and our score function. To do this we: (1) define a reward function that (2) induces a value function, which (3) matches our score function. We now follow these steps.

(1) In MRPs, rewards are defined over edges (transitions); in our setup, scores are defined over nodes (states). We add a “null” child N_u for every node u in the event tree. This null node represents the subset of interventions that do not result in additional events after S_u . In terms of MRPs, there are terminal states. We also assume that every Markov chain will result in a terminal absorbing state. Then, we set the reward function as 1 for a transition from a node u that solves the goal and its null child N_u and 0 otherwise, $R(N_u|u, u \text{ satisfies } g) = 1$, Otherwise $R = 0$.

(2) This reward function induces a value function. Lets denote it with V^{MRP} .

(3) We now show that V^{MRP} is equivalent to the value function presented in the paper V . Specifically, we now prove that

$$V^{MRP} = Pr(u \text{ satisfies } g) = V \quad (17)$$

Proof. Set $\gamma = 1$. Recall that $fr(u', u)$ represents the transition probability from state u to u' . We consider two cases.

(a) If S_u doesn't satisfy g , we have, for every u' ,

$$V^{MRP}(u) = \sum_{u' \text{ child of } u} fr(u', u) \cdot (R(u'|u) + V(u'))$$

where we used recursion and the rule of total probability.

(b) If S_u satisfies g , every descent of u satisfies g . Consider the subtree T_u rooted at u , namely, the subtree containing u and all its descendants. We prove that $V^{MRP}(u) = V(u) = 1$ by induction on the depth of T_u . If the depth= 1, then the graph contains the single edge (u, N_u) , and by definition

$$V^{MRP}(u) = R(N_u|u) + V(N_u) = 1 = V(u).$$

For a general tree depth k , we have an expression similar to the previous case:

$$V^{MRP}(u) = \sum_{u' \text{ child of } u} fr(u', u) \cdot (R(u'|u) + V(u')) \quad (18)$$

$$= fr(N_u, u)R(N_u|u) + \sum_{u' \text{ child of } u, u' \neq N_u} fr(u', u)V(u') \quad (19)$$

$$= \sum_{u' \text{ child of } u} fr(u', u) \quad (20)$$

$$= 1 = V(u) \quad (21)$$

Where the transition from Eq. 19 to Eq. 20 is based on $R(N_u|u) = 1$ by definition. Eq. 21 follows as u' satisfies g , and $T_{u'}$ has depth less than k . Therefore, according to the induction hypothesis $V(u') = 1$. \square

This shows the parallels between our approach and MRPs. Let us also highlight the benefits of our approach in representing the problem.

First, our approach provides a direct way to learn the score (value) function, leveraging the problem's structure. Second, it allows us to incorporate counterfactual information into the cascading process structure using a natural formulation.